Published in final edited form as:
Cytometry A. 2011 October ; 79(10): 855–865. doi:10.1002/cyto.a.21128.

In vivo plant flow cytometry: A first proof-of-concept

Dmitry A. Nedosekin[1], **Mariya V. Khodakovskaya**[2,3], **Alexandru S. Biris**[2,4], **Daoyuan Wang**[2,4], **Yang Xu**[2,4], **Hector Villagarcia**[2], **Ekaterina I. Galanzha**[1], and **Vladimir P. Zharov**[1,*]

[1]Phillips Classic Laser and Nanomedicine Laboratories, Winthrop P. Rockefeller Cancer Institute, University of Arkansas for Medical Sciences, Little Rock, Arkansas 72205, USA

[2]Department of Applied Science, University of Arkansas at Little Rock, Arkansas, 72204, USA

[3]Institute of Biology and Soil Science, Far-Eastern Branch of Russian Academy of Sciences, Vladivostok, 690022, Russia

[4]Nanotechnology Center, University of Arkansas at Little Rock, Arkansas, 72204, USA

Abstract

In vivo flow cytometry has facilitated advances in the ultrasensitive detection of tumor cells, bacteria, nanoparticles, dyes, and other normal and abnormal objects directly in blood and lymph circulatory systems. Here, we propose *in vivo* plant flow cytometry for the real-time noninvasive study of nanomaterial transport in xylem and phloem plant vascular systems. As a proof of this concept, we demonstrate *in vivo* real-time photoacoustic monitoring of quantum dot-carbon nanotube conjugate uptake and uptake by roots and spreading through stem to leaves in a tomato plant. In addition, *in vivo* scanning cytometry using multimodal photoacoustic, photothermal, and fluorescent detection schematics provided multiplex detection and identification of nanoparticles accumulated in plant leaves in the presence of intensive absorption, scattering, and autofluorescent backgrounds. The use of a portable fiber-based photoacoustic flow cytometer for studies of plant vasculature was demonstrated. These integrated cytometry modalities using both endogenous and exogenous contrast agents have a potential to open new avenues of *in vivo* study of the nutrients, products of photosynthesis and metabolism, nanoparticles, infectious agents, and other objects transported through plant vasculature.

Keywords

Photothermal; photoacoustic; flow cytometry; scanning cytometry; imaging; plants; tomato; nanotechnology

INTRODUCTION

Studies of plant-nanoparticle interaction are extremely important to assess the impact of fast-growing nanotechnology products on the environment and agriculture (1,2). Nanomaterials are able to enter into plant cells through cell membranes (3-5) and into the whole plant through roots and plants vascular system (Fig. 1A) inducing changes in plant physiology and gene expression (1,3-9). The accumulation of nanoparticles in plants, especially, in edible ones (6,8), may result in human exposure to these materials. The growing volume of nanomaterials production increases concern over the safety of these nanomaterials to the environment (10). Various novel applications directly oriented to the use of nanotechnology in plants were proposed: delivery of biological molecules into plant

*Address correspondence to: **phone:** +1(501)603-1213 **fax:** +1(501)603-8029 ZharovVladimirP@uams.edu .

cells (4,11), improving herbicide application (12), and enhancing seed germination and plant growth (4,7). Despite this growing number of applications a methodology for studying fate of nanoparticles in plants *in vivo* is still lacking. Existing methods of nanoparticle detection in plants require sample decomposition (8,9,13), and the use of complex methods like transmission electron microscopy (9,14). Magnetic resonance imaging (15) can be used for magnetic nanoparticles only. Main methods for assessment of nanoparticles penetration kinetics include periodic collection of stem and petiole samples from various plants (14,16) and the use of invasive analysis methods. Thus, currently there are no methods available for detection of nanoparticles of various types, their quantification, high-resolution mapping (6), and real-time noninvasive monitoring of live plant tissues (2,15,17).

In biomedical applications various techniques based on optical properties of nanoparticles were developed for noninvasive detection and quantification of nanomaterials in live tissues. For real-time detection of nonfluorescent nanoparticles in blood and lymph, we proposed *in vivo* flow cytometry based on the multiplex integration of photothermal (PT) (18-20), photoacoustic (PA) (20-26), Raman (27,28), and scattering (29) detection techniques. PT and PA flow cytometry (PTFC and PAFC, respectively) methods are based on nonradiative transformation of the absorbed laser energy into heat and acoustic oscillations caused by the fast thermal expansion of the sample. These phenomena are detected either through the changes in optical parameters of the sample or by an ultrasound transducer attached to its surface, respectively. We have demonstrated applications of this noninvasive technique for real-time monitoring of blood cells in different functional states (e.g., normal, apoptotic, and necrotic), circulating tumor cells (melanoma, breast, squamous), bacteria (e.g., Escherichia coli and Staphylococcus aureus), and various nanoparticles and dyes in blood and lymph flow (20–26,30). Scanning PT/PA cytometry was used for the nanoparticles quantification and imaging of tissue samples *in vitro* and *in vivo* (23,24,31). Other groups have explored various modifications of the fluorescent methods which have shown promise in the detection of labeled hematopoietic stem cells, GFP-expressing cells, and tumor cells. Nevertheless, the application of fluorescence-based technology still needs to overcome such challenges as fluorescent tags' cytotoxicity, undesirable immune response to the tags, and low depth of penetration (below 200 μm), allowing to assess small (50–100 μm) superficial microvessel only with slow flow (32-38).

Herewith, we introduce *in vivo* plant flow cytometry for real-time analysis of nanoparticle transport in plants and demonstrate integration of the method with the multispectral scanning cytometry that we have previously developed (6,31). The main goal of *in vivo* plant flow cytometry is to provide a real-time detection of objects transported by the plant vascular system (2). A natural long-distance transport in plants occurs in xylem or phloem tissues (Fig. 1A). Water and nutrients consumed by roots from soil are transported by xylem to the leaves, whereas phloem moves photosynthates, amino acids, and electrolytes originating in the leaves to the rest of the plant (17). For large tomato plants, the average linear flow velocity in xylem was reported to be 8 and 2 mm/s during the day and night hours, respectively (17). In phloem the flow is osmotically generated by the gradient in solutes concentration (39), the corresponding flow velocity was reported to be in the range from 0.2 to 0.4 mm/s (17). As it has been demonstrated previously (6-8), nano-sized materials are able to enter plant roots (Fig. 1B). Possible mechanisms include a standard osmotic pressure-driven transport through the pores that are present in cell walls and intercellular plasmadesmata, or via the highly regulated symplastic transfer (9). Thus, plants may uptake nanoparticles, transport them through xylem, and finally accumulate these nanomaterials in various tissues.

To prove the concept of *in vivo* flow cytometry in plants, we addressed two aspects of plant-nanoparticle interaction: kinetics of nanoparticle uptake and nanoparticle accumulation in

tissues. Uptake kinetic was studied in real time by *in vivo* PA plant flow cytometry, while PT/PA scanning cytometry was used to detect nanoparticles accumulated in various tissues (Fig. 1C). For this study, we selected quantum dot (QD)-carbon nanotube (CNT) conjugates as triple (PT, PA, and fluorescent) contrast agents (40). QDs are typically used as contrast agents for fluorescent imaging (40–43). CNTs have found applications in PT therapy (44), *in vivo* blood and lymph PAFC (21,25,27), and PA tomography (45,46). The conjugation of QDs with CNTs combines the high-fluorescence quantum yield associated with QDs (43) and the strong light absorption of CNTs. Such contrast agents for integrated PT-PA-fluorescent techniques could represent a new and powerful approach for studying the impact of nanotechnology on the environment and agriculture and provided data for comparing in plants application of the listed detection approaches.

METHODS

QD-CNT conjugates

Synthesis—Single-walled CNTs (hereinafter referred to as CNTs) were synthesized over the Fe-Co/MgO catalyst using the RF-CCVD method and methane as the carbon source (47-49). Next, CNTs were functionalized with NH_2 groups through a three-stage treatment: formation of CNT-COOH groups in H_2SO_4/HNO_3 (3:1), followed by $SOCl_2$ treatment that produced CNT-COCl groups, and final reaction with ethylene diamine that gave CNT-NH_2 product. Water-soluble QDs with a CdSe core and a ZnS shell were synthesized according to established protocol (50) and were functionalized with mercaptopropionic acid (MPA) (51,52). The conjugation of CNT-NH_2 and QDs-MPA was performed in aqueous solution (53) with the final (weight/weight) ratio of QDs/CNTs set as 1:100. The coupled QD-CNT conjugates (referred as QDCNTs) were found to be stable: no evidence of QD-CNTs breaking apart was found after intensive sonication.

Instrumentation—The high-resolution transmission electron microscope (HR TEM JEM-2100F, JEOL Inc.) at an acceleration voltage of 200 kV was used for imaging QDs on a surface of CNTs (Fig. 2B). The UV-Vis-NIR optical absorption spectra of the samples (Fig. 2D) were recorded in 1 cm path length quartz cells by using a Shimadzu double-beam spectrophotometer UV-3600 with three detectors. The fluorescent emission of QD-CNTs (Fig. 2D) and the QDs' quantum yield (QY) were determined with the use of Varian Cary Eclipse Fluorescence Spectrophotometer and Rhodamine B/ethanol solution (QY of 0.95 in ethanol) as a comparative standard (54). Samples in 1 cm cuvette were excited at 344 nm, and fluorescent light was collected in the wavelength range of 580 to 620 nm.

Plant model system

Tomato seeds were surface-sterilized, germinated, and grown on sterile Murashige and Skoog (MS) medium as previously described (6). 30-day-old tomato plants (cv. Micro-Tom) with an average stem length of 5-10 cm were used in all the experiments.

The kinetic of QD-CNTs uptake from the water was monitored *in vivo* in intact tomato plants transferred from agar medium to a tube with regular water. First group (3 plants) remained in the water throughout the entire experiment (control). A second group ($n = 9$) was used to monitor the flow of QD-CNTs inside the plants tissues (experimental plants). Control PA signals (in the absence of QD-CNTs) were acquired from control plants and from experimental plants before the introduction of nanoparticles. After the control recordings 200 μL of 25 μg/ml QD-CNT solution were added to the water in a tube containing the plant (Fig. 1B) and PA signals were recorded for 1 hour from the mid-vein of a leaf or from the main stem. Experiments were repeated for each tomato plant serving as independent biological replicate.

Accumulation of QD-CNTs in tomato plants was studied with a focus on leaf examination in 30-day-old plants grown for 10 days on a MS medium supplemented with QD-CNTs (at a concentration of 50 lg/ml). Leaves of tomato plants grown on a standard MS medium were used as a control (total 6 leaves from three different plants); for each leaf from 1 to 3 areas with a size of 500×500 μm were analyzed to estimate background PT/PA signals. A tomato leaf was prepared for microscope calibration by local injection of 30 ll of a 0.5 mg/ml QD-CNT solution into the leaf tissues. For imaging convenience whole tomato leaves were detached from a stem and deposited for observation on a glass slide under a coverslip (Fig. 3C).

Integrated plant cytometer

The prototype of a plant cytometer (Fig. 3A) was built on the technical platform of an Olympus invert IX81 microscope (Olympus America, Inc., Center Valley, PA) with incorporated scanning PT/PA setup, PA flow cytometer, and conventional fluorescent wide-field imaging module.

Scanning PT/PA microscope-cytometer implemented a tunable optical parametric oscillator (OPO, Opolette HR 355 LD, OPOTEK, Carlsbad, CA) with the following parameters: tunable wavelength range, 420 to 2,500 nm; pulse width, 5 ns; pulse repetition rate, 100 Hz; and beam diameter on sample, 1.2 lm. XY translation stage (H117 ProScan II, Prior Scientific, Rockland, MA) was used for raster scanning of the plant sample (Fig. 3C). The PT (also referred to as thermal-lens) effect was manifested by defocusing a probe He-Ne laser beam (wavelength, 633 nm; power, 1.4 mW; model 117A, Spectra-Physics, Santa Clara, CA) at a photodetector (PDA36A, 40 dB amplification, ThorLabs, Newton, NJ) pinhole pane after the sample. The PT signal showed the linear positive asymmetric component associated with fast heating and slower cooling effects and a nonlinear sharp negative peak associated with nano-bubble formation around the overheated zones (Fig. 4C) (22). PA effect or laser-induced acoustic waves in the sample were detected by an ultrasound transducer (XMS-310, Panametrics-NDT, Olympus NDT, Center Valley, PA) and amplified (preamplifier model 5662B; bandwidth, 50 kHz–5 MHz; gain 54 dB; Panametrics NDT, Olympus NDT Inc., Center Valley, PA). The transducer was placed directly onto a sample with water used to improve acoustic coupling. The PA signal had a classic bipolar shape transformed into a pulse train due to reflections and diffraction effects (Fig. 4D).

In vivo PA plant flow cytometer was equipped with a high pulse rate Yb-doped fiber laser (MOPA-M-10, MultiWave Photonics, Portugal) with the following parameters: wavelength, 1064 nm; pulse width, 10 ns; pulse repetition rate, 10 kHz - 0.5 MHz; energy fluence range on sample surface, 0.01 – 1.0 J/cm^2. Laser radiation was delivered either through the microscope based setup described above or through a 400 μm multimode fiber (M28L05, Thorlabs, Newton, NJ) with a custom miniature tip featuring cylindrical optics (Fig. 3B). Both the transducer and the optical-fiber tip were fixed in a holder and were gently touching the plant stem (Fig. 3D). For both the microscope based setup and for the fiber tip the laser beam spot in the sample had linear shape with the dimensions of 200 X 150 and 50 X 400 μm, respectively.

The analysis of PT and PA signal was performed by a PC (Dell Precision 690) equipped with a high-speed (200 MHz) analog-to-digital converter board PCI-5124 (National Instruments, Austin, TX) which was used to acquire signals from the transducer and photodiode. Control over the setup and signal acquisition/procession was realized via a custom software module (LabView 8.5 complex, National Instruments, Austin, TX). PT/PA images were constructed by plotting PT/PA signal amplitude in a XY coordinate plane with the gray shading used to represent the signal amplitude. All the PT/PA signals with the

amplitudes not exceeding 5σ level (five times the standard deviation of the background signal in the absence of the excitation beam) were plotted in a black color.

Fluorescent wide-field imaging of the QDs was performed with a custom filter: excitation 450 ±40 nm, emission 600 ± 8 nm, and a single band dichroic 510 nm (Semrock, Inc. Rochester, NY). Exposure of fluorescent imaging was 200 ms for leaves and 5 s for roots. For leaves 200 ms exposure corresponded to a "black" image of a control plant leaf (the maximal image pixel intensity below 5/256 level in a greyscale mode). This exposure duration was selected experimentally as the shortest one for a set of leaves images taken for 5 different control plants. The fluorescent spectra of the samples were obtained by spectrophotometer (USB4000, Ocean Optics, Dunedin, FL) with a fluorescent filter featuring a long-pass emission filter transmitting light with wavelengths longer than 600 nm (Semrock, Inc. Rochester, NY). The optical transmission and fluorescent images of selected plant parts were obtained with a color CCD camera (DP-72, Olympus, Center Valley, PA).

Statistical analysis

Results were expressed as means plus/minus the standard error of at least three independent experiments. Results for independent biological replicates were compared by unpaired T-test. $P < 0.05$ was regarded as statistically significant. In PAFC mode the increase in PA signal amplitude exceeding 5σ criterion (five times standard deviation of the baseline) was considered statistically significant, i.e. corresponding to QD-CNTs. Statistica 5.11 software (StatSoft, Inc.,USA) and MATLAB 7.0.1 (MathWorks) were used for the statistical calculations.

RESULTS

Characterization of QD-CNTs

Hybrid nanoparticles synthesized by conjugation of QDs and CNTs were selected for verification of the *in vivo* plant flow and scanning cytometry modalities. The success of conjugation was proved by TEM imaging (Fig. 2B) that demonstrated the presence of multiple QDs on the exterior surface of the CNTs — some of them formed small bundles. Absorption spectrum of QD-CNTs slightly differed from that of pure CNTs (Fig. 2D), featuring small increase at the wavelengths corresponding to the QDs' absorption maximum. The fluorescence microscopy demonstrated intensive fluorescence of QD-CNTs aggregates (Fig. 2C).

At the first stage of *in vitro* tests we characterized multimodal imaging of QD-CNT conjugates to assess possible changes in imaging contrast due to formation of complex nanoprobes (Fig. 3A). Large QD-CNT aggregates were successfully imagined *in vitro* as by transmission microscopy, so as by fluorescent and photothermal modalities (Fig. 4A). Detection limits for fluorescent and PT detection were estimated to be at the level of 200 nm cluster for both methods. Calibration graph based on fluorescent imaging data (Fig. 4A, bottom right) revealed fluorescence quenching (53,55,56) in large QD-CNT aggregates. Comparison of QD-CNT conjugates with aggregates of pure QDs (2-5 μm sized clusters, Fig. 4B) revealed approximately 3 folds decrease in fluorescence intensity for the aggregates of the same size. The experiments with Rhodamine B/ethanol solution as a comparative standard also confirmed the decrease in quantum yield from 30% to 7.8% for QDs attached to CNTs.

The calibration graph for PT detection was linear up to 5μm QD-CNT aggregates. With the increase in aggregate size or at higher laser energy, the nonlinear PT signal amplification was observed. The light absorption of individual QDs in near-infrared (NIR) range selected for plants imaging was relatively low. At the wavelength of 590 nm corresponding to QDs

absorbance maximum signal-to-noise ratio (SNR) was in the range of 4-8 for 500 μm clusters. Thus, even though QDs have sufficient optical contrast for PT detection (40), QDs absorbance in NIR range can be ignored in PT/PA plants studies. A comparison of the amplitudes and, especially, the shapes of PT/PA signals for CNT and QD-CNT clusters (Figs. 4C and 4D) under similar conditions confirmed the that conjugation did not affected PT/PA contrast of QD-CNTs, which was in line with the spectroscopic data (Fig. 2D). As expected, fluorescent intensity of pure CNTs was undetectable under conditions selected.

Thus, the conjugation of QDs and CNTs produced hybrid nanoprobes suitable for PA and PT detection as for fluorescent imaging. The PT and PA contrast of the nanoparticles was not changed, however, the fluorescent intensity decreased two to threefold. Fluorescence quenching was observed for large aggregates of QD-CNTs, probably, due to excitation and emission photons absorption by CNTs.

In vivo plant flow cytometry of QD-CNTs in tomato vascular system

To study kinetics of nanoparticle uptake by a plant we proposed the use of a PAFC, which provided unique integration of the high sensitivity and noninvasive analysis in thick tissues. In PAFC mode a laser beam was focused into the vessel and interacted with light-absorbing objects transported through plant vasculature (xylem or phloem). The laser wavelength (1064 nm) was selected to minimize background signal of the plant tissues. Fast heating of the circulating objects (Fig. 1C, red) by absorbed laser irradiation provided generation of acoustic waves (21) in a result of a fast thermal expansion (PA effects).

First, transport of QD-CNTs through plant vasculature was monitored by PAFC in the leaf mid-vein (Fig. 5A). Close to the petiole, the linear flow velocity was expected to be as high as in the petiole, while leaf structures are thinner than those of a petiole or stem. A microscope was used for precise navigation and focusing of the laser beam onto the vein (Fig. 5A). For the control plants, there were no PA signals with amplitude exceeding 5r threshold level. PA signals exceeding this level were observed at 5 ± 1.3 min (n = 5) after the QD-CNTs were added to the water (Fig. 5B). In all of the experiments, we observed rare PA signals indicating the presence of nanoparticles in plant vasculature (Fig. 5B). The number of PA peaks observed and the appearance rate varied for different individual plants (replicates) and was in a range from 2 to 15 peaks per 30 min. Based on our previous experience with PA detection of circulating CNTs in blood and lymph flow (21,22,25) low PA signals could be associated with individual QD-CNTs and large nonlinear PA signals corresponded to 2-5 lm aggregates. Taking into account the average distance between the roots and the detection point (~ 5 cm), as well as the observed appearance delay of 5 min, the average linear flow velocity can be estimated as 0.2 mm/s—which does not contradict data available in the literature (17).

Secondly, the PA signals were monitored in the plant stem using optical-fiber to deliver laser radiation (Fig. 3B). As xylem bundles are arranged symmetrically around the stem center (Fig. 1C), a fiber tip can easily be positioned against any part of the stem. In the stem, which was thicker than the leaf, laser radiation at 1064 nm was better absorbed by deep stem structures. The level of background PA signals was increased 3 - 5-folds from 2 - 4 mV for a leaf vein to a 10 - 20 mV level for a stem. In addition, the scattering and attenuation of the laser beam in stem tissues led to a decrease in laser fluence, thus, further decreasing sensitivity. Nevertheless, PAFC provided detection of QD-CNTs transported through the stem. As can be seen from the PA trace (Fig. 5C), the first detectable QD-CNTs reached the detection point in as few as 10 min (mean 14 ± 3 min, n = 4) compared to an average of 5 min for detection in mid-vein leaves despite shorter travel path from roots to detection zone in a stem.

Thus, PAFC revealed presence of QD-CNTs in plant vasculature. The data obtained in the leaves and in the stems indicate presence both of individual CNTs and of clustered QD-CNTs in xylem flow (Fig. 5). The lower PA background in the leaves provided better conditions for detection of QD-CNTs.

Scanning cytometry of QD-CNTs accumulated in tomato roots and leaves

Scanning cytometry was used to analyze spatial distribution of QD-CNTs escaped from vascular system into tomato leaves. Their detection in plant tissues and distribution mapping were performed by integrated wide-field fluorescent, PT, and PA techniques (Fig. 1C, bottom) to: 1) confirm the presence of QD-CNTs in various plant tissues, 2) analyze the distribution patterns for accumulated nanoparticles, and 3) to demonstrate the improvement in detection accuracy by matching fluorescence of QD with PT/PA signature of a CNT.

The autofluorescence background from leaves (Fig. 1A) and roots affected fluorescent imaging of QD-CNTs. Tomato leaves autofluorescence in the red spectral range was associated mainly with plant chlorophylls (Fig. 2E) and had two maxima near 690 nm and 740 nm (57). The selection of a narrow band filter in the spectral range of maximal QDs emission (600 ± 8 nm) increased QDs contrast over plant tissues. Indeed, some bright fluorescent spots were observed apart from the vascular vessels in plants grown on QD-CNT-containing MS medium (Fig. 6A). QD-CNT clusters with an average size in the range of 5 - 15 μm. The majority of these clusters were observed in leaf tissues close to a vasculature. The identification of small QD-CNT clusters in tomato leaves with the fluorescent imaging was difficult due to a very heterogeneous background and the possible attenuation of QDs optical emission by plant tissues. In the roots of tomato plants, we were able to identify QD-CNT clusters as small as 2 μm (Fig. 6B). Compared to thick leaf structures, light-scattering and attenuation in roots are much lower. Thus, fluorescent wide-field imaging of QD-CNTs in plants alone was not sufficient for identification of nanoparticles (due to high heterogeneity of plant autofluorescence).

Next, PT/PA scanning cytometry was used to confirm that bright spots discovered in the sample indeed were QD-CNTs. The near-infrared (NIR) spectral range of 750-950 nm was considered as the most promising for PT/PA plant cytometry as the absorption background from chlorophyll and other plant components in the NIR range is much lower than that in the visible range (Fig. 2E), while the absorption of QD-CNTs decreases only two-three fold in the NIR range compared to that in visible range (Fig. 2D). Moreover, the sensitivity of PT/PA cytometry was enhanced by laser-induced nano- and micro-bubbles around laser-overheated QD-CNT clusters (25,31) acting as PT/PA signal amplifiers (Fig. 4C-D). In particular, the bubbles' expansion and collapse take several microseconds leading to the formation of sharp, negative PT signals as signatures of the strong local absorption associated with QD-CNT clusters (Fig. 4C).

For calibration purposes, a solution containing QD-CNTs was injected into the leaf tissues (Fig. 7A), while another leaf was inoculated with pure CNTs at a similar concentration. These areas were imaged by PT/PA scanning cytometer. The locations of the signals correlated with the incision sites for both CNTs and QD-CNTs. Imaging contrast (as a ratio of signal amplitude from nanoparticles to tissue background) for QD-CNT clusters were in the range of 30 – 40 and 5 – 10, for PT and PA detection, respectively, confirming higher sensitivity of PT detection in thin leaves. The PT images (Fig. 7C) were well-correlated with fluorescence images of the QD-CNTs among the leaf structures (Fig. 7B). There were no PT/PA signals exceeding control signal level acquired from the leaf vascular tissues, which provided a strong background in the fluorescent images (see blue arrows, Figs. 7A-C).

Two approaches to the use of a PT/PA scanning cytometry for QD-CNTs detection in the leaves of a plant grown on nanomaterial-containing medium were tested: 1) imaging of a small area having abovementioned fluorescing features and 2) imaging of a larger sample area (up to 1×1 mm) having no distinctive fluorescent features. In the first case, we observed high PT/PA signals (SNR in the range of 20-30 similar to those observed for a phantom sample) collocated with the fluorescent artifacts in the sample (Figs. 7D and 7E). High PT/PA signals were observed for 13 sites out of 17 scanned indicating that 4 sites were identified as containing QD-CNTs incorrectly. Both the amplitudes and the shapes of the PT signals revealed specific features (Fig. 4C) associated with nano- and micro-bubbles' formation around aggregated QD-CNTs. PT imaging of the leaves with no substantial fluorescent signatures (exceeding the level of heterogeneity observed for control plants) revealed presence of multiple PT/PA signals (Fig. 7F) featuring shapes and amplitudes specific to nanomaterials. SNR for observed PT signals was in the range of 5-10, suggesting that much smaller aggregates were detected than in the case of a phantom. These aggregates could be related either with smaller size or with particles deposition in deeper plant tissues, i.e. with fluorescence scattering and quenching. PT imaging revealed very high heterogeneity of nanomaterials distribution in the sample with the highest density of detected nanomaterials along the main vascular veins (Fig. 7F) and much fewer particles found in areas with only small capillaries. For a typical leaf area of 500×500 μm there were 27±12 (n = 7) and 4±3 (n = 4) PT/PA signals detected near a large vein and near edge of the leaf, respectively.

Thus, PT/PA cytometry confirmed the presence of accumulated nanoparticles and demonstrated higher sensitivity in detection of smaller aggregates in plant tissues compared to fluorescence imaging.

DISCUSSIONS

In this paper we have presented an integrated fluorescence/PT/PA cytometry in plant tissues developed with a focus on study nanoparticles uptake kinetics and detection of nanomaterials accumulated in plants. To the best of our knowledge, this is the first demonstration of *in vivo* non-invasive detection of the nanomaterials accumulated in plant tissues or transported by plant vascular tissues. PA/PT based cytometry can be applied to a wide range of nanomaterials, have high sensitivity sufficient for detection of even individual nanoparticles and can be applied for vascular flow monitoring. The experiments in tomato plants demonstrated feasibility of in vivo PA/PT based cytometry with a potential to detect nanomaterials, viruses, bacteria, and other plant disease-associated pathogens or tumor cells (62) in both phloem and xylem tissues, and in vascular system. In Table 1 we summarized potential applications of PT/PA based methods.

PAFC proved to be a robust platform for routine testing ecotoxicological risks of nanomaterials through a rapid and accurate assessment of uptake kinetics. The method is express, simple, and shows potential application with virtually any plant and for a wide range of nonfluorescent nanomaterials. The study of viruses, bacteria and other pathogens transported through vascular tissues of plants may use the principles of *in vivo* PAFC in mammalians (21): labeling of objects of interest with functionalized nanoparticles (24) followed by PAFC detection of these labels in the plant. The analysis of transportation dynamics revealed feasibility of another PAFC application for vascular flow velocity studies as on a large scale (presented here roots-leaves transportation by xylem), so as ultralocal flow rate measurement by PA time-of-flight technique (23,25). The applications listed here are feasible not only on a lab bench, but also could be transferred into a field with a use of a portable fiber laser cytometer presented. In-field applications of PAFC could include rapid, sample preparation free screening of live plants for presence of nanomaterials in vascular

tissues in the case of anthropogenic contamination. One of the main advantages of PAFC *in vivo* plant flow cytometry is noninvasive detection and deep tissues assessing. This eliminates limitations on a plant size and makes it possible to avoid flow disturbances usually associated with invasive xylem liquid collection methods. For the large plants and thick tissues PAFC sensitivity is decreased due to a high level of background PA signal. However, this drawback can be minimized either by the use of a focused transducer rejecting out-of-focus acoustic waves or by the local laser bleaching of plant chromophores around the detection zone by the use of high energy laser pulses (6).

Scanning fluorescent/PT/PA cytometry provides an opportunity to reveal the fate of nanomaterials penetrated into a plant. First, for nanomaterials having a high fluorescent quantum yield the fluorescent imaging is an obvious choice. However, intensive and heterogeneous autofluorescence of plant tissues decreases imaging contrast and identification accuracy. Such fluorescent techniques like spectral deconvolution, multispectral imaging and confocal imaging could be used to separate fluorescence of nanomaterials from autofluorescence of plant tissues and enhance imaging contrast. Still, fluorescent imaging in plants has the same drawbacks as in mammal tissues: the need to consider autofluorescent background and low depth of penetration of fluorescent photons. Second, various nanomaterials like gold nanospheres, gold nanorods, carbon nanotubes, etc. have very high light absorbance. Integration of two modalities in a single scheme provides a highly sensitive detection in optically thin samples (≤ 100 μm) by the means of PT detection scheme and analysis in deep tissues with a PA mode. Indeed, the PA technique which is insensitive to scattering background has already demonstrated the possibility of deep tissue imaging in animals (depth penetration of 3-5 cm) (40,43,46) and, as we show here, translation of this schematic to plants is feasible. Nonlinear thermal effects occurring upon absorption of the high energy laser pulses by nanomaterials provide a unique approach to identification of nanomaterials in the plant tissues.

In the current experimental setup, scanning of a small area 100–400 μm in diameter takes approximately 2-10 min. The imaging of a larger area (1×1 mm) with high resolution can take up to one hour. Future development of PT/PA scanning cytometry we envision as combination of a high pulse repetition rate laser sources (up to 500 kHz (25)) with an optical scanning systems (63). Multispectral PT/PA imaging and spectral analysis is also feasible with the use of successive laser pulses of different wavelengths slightly separated in time (23).

Acknowledgments

This work was supported in part by the National Institute of Health, grant numbers R01CA131164, R01 EB009230, and R21CA139373 (VPZ), the National Science Foundation, grant numbers DBI-0852737 (VPZ), and Department of Defense grants: W88XWH-10-2-0130, W81XWH-10-BCRP-CA, and W81XWH-11-1-0129. Funding from ASTA (grant # 08-CAT-03) is highly appreciated (ASB). Funding from the Arkansas Space Consortium (Award UALR19845) is highly appreciated (MVK). The authors acknowledge the help of Dr. Marinelle Ringer (UALR) in editing this manuscript.

References

1. Joseph, T.; Morrison, M. Nanotechnology in agriculture and food. 2006. www.nanoforum.org
2. Ma X, Geiser-Lee J, Deng Y, Kolmakov A. Interactions between engineered nanoparticles (ENPs) and plants: Phytotoxicity, uptake and accumulation. Science of The Total Environment. 2010; 408:3053–3061. [PubMed: 20435342]
3. Etxeberria E, Gonzalez P, Baroja-Fernandez E, Romero J Pozueta. Fluid phase endocytic uptake of artificial nano-spheres and fluorescent quantum dots by sycamore cultured cells. J Plant Signaling Behav. 2006; 1:196–200.

4. Liu QL, Chen B, Wang QL, Shi XL, Xiao ZY, Lin JX, Fang XH. Carbon nanotubes as molecular transporters for walled plant cells. Nano Lett. 2009; 9:1007–1010. [PubMed: 19191500]
5. Stampoulis D, Sinha SK, White JC. Assay-dependent phytotoxicity of nanoparticles to plants. Environ Sci Technol. 2009; 43:9473–9479. [PubMed: 19924897]
6. Khodakovskaya MV, de Silva K, Nedosekin DA, Dervishi E, Biris AS, Shashkov EV, Galanzha EI, Zharov VP. Complex genetic, photothermal, and photoacoustic analysis of nanoparticle-plant interactions. Proc Natl Acad Sci USA. 2011; 108:1028–1033. [PubMed: 21189303]
7. Khodakovskaya M, Dervishi E, Mahmood M, Xu Y, Li ZR, Watanabe F, Biris AS. Carbon nanotubes are able to penetrate plant seed coat and dramatically affect seed germination and plant growth. Acs Nano. 2009; 3:3221–3227. [PubMed: 19772305]
8. Zhu H, Han J, Xiao JQ, Jin Y. Uptake, translocation, and accumulation of manufactured iron oxide nanoparticles by pumpkin plants. J Environ Monit. 2008; 10:713–717. [PubMed: 18528537]
9. Lin SJ, Reppert J, Hu Q, Hudson JS, Reid ML, Ratnikova TA, Rao AM, Luo H, Ke PC. Uptake, Translocation, and Transmission of Carbon Nanomaterials in Rice Plants. Small. 2009; 5:1128–1132. [PubMed: 19235197]
10. Tiede K, Hassellöv M, Breitbarth E, Chaudhry Q, Boxall ABA. Considerations for environmental fate and ecotoxicity testing to support environmental risk assessments for engineered nanoparticles. Journal of Chromatography A. 2009; 1216:503–509. [PubMed: 18805541]
11. Torney F, Trewyn BG, Lin VSY, Wang K. Mesoporous silica nanoparticles deliver DNA and chemicals into plants. Nat Nanotechnol. 2007; 2:295–300. [PubMed: 18654287]
12. Perez-de-Luque A, Rubiales D. Nanotechnology for parasitic plant control. Pest Manag Sci. 2009; 65:540–545. [PubMed: 19255973]
13. Doshi R, Braida W, Christodoulatos C, Wazne M, O'Connor G. Nano-aluminum: Transport through sand columns and environmental effects on plants and soil communities. Environmental Research. 2008; 106:296–303. [PubMed: 17537426]
14. Corredor E, Testillano P, Coronado M-J, Gonzalez-Melendi P, Fernandez-Pacheco R, Marquina C, Ibarra MR, de la Fuente J, Rubiales D, Perez-de-Luque A. Nanoparticle penetration and transport in living pumpkin plants: in situ subcellular identification. BMC Plant Biology. 2009; 9:45. others. [PubMed: 19389253]
15. Huang X, Stein BD, Cheng H, Malyutin A, Tsvetkova IB, Baxter DV, Remmes NB, Verchot J, Kao C, Bronstein LM. Magnetic Virus-like Nanoparticles in N. benthamiana Plants: A New Paradigm for Environmental and Agronomic Biotechnological Research. Acs Nano. 2011; 5:4037–4045. others. [PubMed: 21452886]
16. González-Melendi P, Fernández-Pacheco R, Coronado MJ, Corredor E, Testillano PS, Risueño MC, Marquina C, Ibarra MR, Rubiales D, Pérez-de-Luque A. Nanoparticles as Smart Treatment-delivery Systems in Plants: Assessment of Different Techniques of Microscopy for their Visualization in Plant Tissues. Annals of Botany. 2008; 101:187–195. [PubMed: 17998213]
17. Windt CW, Vergeldt FJ, De Jager PA, Van As H. MRI of long-distance water transport: a comparison of the phloem and xylem flow characteristics and dynamics in poplar, castor bean, tomato and tobacco. Plant, Cell Environ. 2006; 29:1715–1729. [PubMed: 16913861]
18. Zharov V, Gaalnzha E, Tuchin V. Photothermal imaging of moving cells in lymph and blood flow in vivo. Proc SPIE. 2004; 5320:185–195.
19. Zharov VP, Galanzha EI, Tuchin VV. Photothermal image flow cytometry in vivo. Opt Lett. 2005; 30:628–630. [PubMed: 15791998]
20. Zharov VP, Galanzha EI, Tuchin VV. In vivo photothermal flow cytometry: Imaging and detection of individual cells in blood and lymph flow. J Cell Biochem. 2006; 97:916–932. [PubMed: 16408292]
21. Zharov VP, Galanzha EI, Shashkov EV, Kim JW, Khlebtsov NG, Tuchin VV. Photoacoustic flow cytometry: principle and application for real-time detection of circulating single nanoparticles, pathogens, and contrast dyes in vivo. J Biomed Opt. 2007; 12
22. Galanzha EI, Shashkov EV, Tuchin VV, Zharov VP. In vivo multispectral, multiparameter, photoacoustic lymph flow cytometry with natural cell focusing, label-free detection and multicolor nanoparticle probes. Cytometry Part A. 2008; 73A:884–894.

23. Galanzha EI, Shashkov EV, Spring PM, Suen JY, Zharov VP. In vivo, noninvasive, label-free detection and eradication of circulating metastatic melanoma cells using two-color photoacoustic flow cytometry with a diode laser. Cancer Res. 2009; 69:7926–7934. [PubMed: 19826056]
24. Galanzha EI, Shashkov EV, Kelly T, Kim JW, Yang LL, Zharov VP. In vivo magnetic enrichment and multiplex photoacoustic detection of circulating tumour cells. Nat Nanotechnol. 2009; 4:855–860. [PubMed: 19915570]
25. Nedosekin DA, Sarimollaoglu M, Shashkov EV, Galanzha EI, Zharov VP. Ultra-fast photoacoustic flow cytometry with a 0.5 MHz pulse repetition rate nanosecond laser. Opt. Express. 2010; 18:8605–8620. [PubMed: 20588705]
26. Zharov VP. Ultrasharp nonlinear photothermal and photoacoustic resonances and holes beyond the spectral limit. Nat Photon. 2011; 5:110–116.
27. Biris AS, Galanzha EI, Li ZR, Mahmood M, Xu Y, Zharov VP. In vivo Raman flow cytometry for real-time detection of carbon nanotube kinetics in lymph, blood, and tissues. J Biomed Opt. 2009; 14:021006. [PubMed: 19405719]
28. Shashkov EV, Galanzha EI, Zharov VP. Photothermal and photoacoustic Raman cytometry in vitro and in vivo. Opt Express. 2010; 18:6929–6944. [PubMed: 20389713]
29. Galanzha EI, Tuchin VV, Zharov VP. In vivo integrated flow image cytometry and lymph/blood vessels dynamic microscopy. J Biomed Opt. 2005; 10:054018. [PubMed: 16292978]
30. Kim JW, Galanzha EI, Shashkov EV, Moon HM, Zharov VP. Golden carbon nanotubes as multimodal photoacoustic and photothermal high-contrast molecular agents. Nat Nanotechnol. 2009; 4:688–694. [PubMed: 19809462]
31. Nedosekin DA, Shashkov EV, Galanzha EI, Hennings L, Zharov VP. Photothermal multispectral image cytometry for quantitative histology of nanoparticles and micrometastasis in intact, stained and selectively burned tissues. Cytometry Part A. 2010; 77A:1049–1058.
32. Novak J, Georgakoudi I, Wei X, Prossin A, Lin CP. In vivo flow cytometer for real-time detection and quantification of circulating cells. Opt Lett. 2004; 29:77–79. [PubMed: 14719666]
33. Georgakoudi I, Solban N, Novak J, Rice WL, Wei XB, Hasan T, Lin CP. In vivo flow cytometry: A new method for enumerating circulating cancer cells. Cancer Res. 2004; 64:5044–5047. [PubMed: 15289300]
34. Boutrus S, Greiner C, Hwu D, Chan M, Kuperwasser C, Lin CP, Georgakoudi I. Portable two-color in vivo flow cytometer for real-time detection of fluorescently-labeled circulating cells. J Biomed Opt. 2007; 12:020507. [PubMed: 17477705]
35. He W, Wang HF, Hartmann LC, Cheng JX, Low PS. In vivo quantitation of rare circulating tumor cells by multiphoton intravital flow cytometry. Proc Natl Acad Sci USA. 2007; 104:11760–11765. [PubMed: 17601776]
36. Tkaczyk ER, Zhong CF, Ye JY, Myc A, Thomas T, Cao Z, Duran-Struuck R, Luker KE, Luker GD, Norris TB. In vivo monitoring of multiple circulating cell populations using two-photon flow cytometry. Opt Commun. 2008; 281:888–894. others. [PubMed: 19221581]
37. Zhong CF, Tkaczyk ER, Thomas T, Ye JY, Myc A, Bielinska AU, Cao Z, Majoros I, Keszler B, Baker JR. Quantitative two-photon flow cytometry - in vitro and in vivo. J Biomed Opt. 2008; 13 others.
38. Chang YC, Ye JY, Thomas TP, Cao ZY, Kotlyar A, Tkaczyk ER, Baker JR, Norris TB. Fiber-optic multiphoton flow cytometry in whole blood and in vivo. J Biomed Opt. 2010; 15
39. Van Bel AJE. The phloem, a miracle of ingenuity. Plant, Cell Environ. 2003; 26:125–149.
40. Shashkov EV, Everts M, Galanzha EI, Zharov VP. Quantum dots as multimodal photoacoustic and photothermal contrast agents. Nano Lett. 2008; 8:3953–3958. [PubMed: 18834183]
41. Kang HG, Tokumasu F, Clarke M, Zhou ZP, Tang JY, Nguyen T, Hwang J. Probing dynamic fluorescence properties of single and clustered quantum dots toward quantitative biomedical imaging of cells. Wiley Interdiscip Rev Nanomed Nanobiotechnol. 2010; 2:48–58. [PubMed: 20049830]
42. Yong KT, Qian J, Roy I, Lee HH, Bergey EJ, Tramposch KM, He SL, Swihart MT, Maitra A, Prasad PN. Quantum rod bioconjugates as targeted probes for confocal and two-photon fluorescence imaging of cancer cells. Nano Lett. 2007; 7:761–765. [PubMed: 17288490]

43. Guo Y, Shi DL, Cho HS, Dong ZY, Kulkarni A, Pauletti GM, Wang W, Lian J, Liu W, Ren L. In vivo imaging and drug storage by quantum-dot-conjugated carbon nanotubes. Adv Funct Mater. 2008; 18:2489–2497. others.
44. Kim JW, Shashkov EV, Galanzha EI, Kotagiri N, Zharov VP. Photothermal antimicrobial nanotherapy and nanodiagnostics with self-assembling carbon nanotube clusters. Laser Surg Med. 2007; 39:622–634.
45. Kim C, Song KH, Gao F, Wang LV. Sentinel lymph nodes and lymphatic vessels: noninvasive dual-modality in vivo mapping by using indocyanine green in rats—volumetric spectroscopic photoacoustic imaging and planar fluorescence imaging. Radiology. 2010; 255:442–450. [PubMed: 20413757]
46. Pramanik M, Swierczewska M, Green D, Sitharaman B, Wang LV. Single-walled carbon nanotubes as a multimodal-thermoacoustic and photoacoustic-contrast agent. J Biomed Opt. 2009; 14:034018. [PubMed: 19566311]
47. Dervishi E, Li ZR, Watanabe F, Xu Y, Saini V, Biris AR, Biris AS. Thermally controlled synthesis of single-wall carbon nanotubes with selective diameters. J Mater Chem. 2009; 19:3004–3012.
48. Biris AS, Schmitt TC, Little RB, Li Z, Xu Y, Biris AR, Lupu D, Dervishi E, Trigwell S, Miller DW. Influence of the RF excitation of the catalyst system on the morphology of multiwalled carbon nanotubes. J Phys Chem C. 2007; 111:17970–17975. others.
49. Xu Y, Li ZR, Dervishi E, Saini V, Cui JB, Biris AR, Lupu D, Biris AS. Surface area and thermal stability effect of the MgO supported catalysts for the synthesis of carbon nanotubes. J Mater Chem. 2008; 18:5738–5745.
50. Sun Q, Wang YA, Li LS, Wang DY, Zhu T, Xu J, Yang CH, Li YF. Bright, multicoloured light-emitting diodes based on quantum dots. Nat Photonics. 2007; 1:717–722.
51. Xu Y, Karmakar A, Wang DY, Mahmood MW, Watanabe F, Zhang YB, Fejleh A, Fejleh P, Li ZR, Kannarpady G. Multifunctional Fe3O4 cored magnetic-quantum dot fluorescent nanocomposites for RF nanohyperthermia of cancer cells. J Phys Chem C. 2010; 114:5020–5026. others.
52. Blackman B, Battaglia D, Peng XG. Bright and water-soluble near IR-Emitting CdSe/CdTe/ZnSe Type-II/Type-I nanocrystals, tuning the efficiency and stability by growth. Chem Mater. 2008; 20:4847–4853.
53. Pan BF, Cui DX, He R, Gao F, Zhang YF. Covalent attachment of quantum dot on carbon nanotubes. Chem Phys Lett. 2006; 417:419–424.
54. Karstens T, Kobs K. Rhodamine-B and rhodamine-101 as reference substances for fluorescence quantum yield measurements. J Phys Chem. 1980; 84:1871–1872.
55. Biju V, Itoh T, Baba Y, Ishikawa M. Quenching of photoluminescence in conjugates of quantum dots and single-walled carbon nanotube. J Phys Chem B. 2006; 110:26068–26074. [PubMed: 17181259]
56. Nikoobakht B, Burda C, Braun M, Hun M, El-Sayed MA. The quenching of CdSe quantum dots photoluminescence by gold nanoparticles in solution. Photochem Photobiol. 2002; 75:591–597. [PubMed: 12081320]
57. Benediktyova Z, Nedbal L. Imaging of multi-color fluorescence emission from leaf tissues. Photosynth Res. 2009; 102:169–175. [PubMed: 19784795]
58. Carbajal D, Morano KA, Morano LD. Indirect Immunofluorescence Microscopy for Direct Detection of Xylella fastidiosa in Xylem Sap. Current Microbiology. 2004; 49:372–375. [PubMed: 15486713]
59. French CJ, Elder M. Virus particles in guttate and xylem of infected cucumber (Cucumis sativus L.). Annals of Applied Biology. 1999; 134:81–87.
60. Gould N, Minchin PEH, Thorpe MR. Direct measurements of sieve element hydrostatic pressure reveal strong regulation after pathway blockage. Functional Plant Biology. 2004; 31:987–993.
61. Minchin PEH, Thorpe MR. Using the short-lived isotope (11)C in mechanistic studies of photosynthate transport. Functional Plant Biology. 2003; 30:831–841.
62. Tanev S, Sun WB, Pond J, Tuchin VV, Zharov VP. Flow cytometry with gold nanoparticles and their clusters as scattering contrast agents: FDTD simulation of light-cell interaction. Journal of Biophotonics. 2009; 2:505–520. [PubMed: 19670359]

63. Krivacic RT, Ladanyi A, Curry DN, Hsieh HB, Kuhn P, Bergsrud DE, Kepros JF, Barbera T, Ho MY, Chen LB. A rare-cell detector for cancer. Proc Natl Acad Sci USA. 2004; 101:10501–10504. others. [PubMed: 15249663]

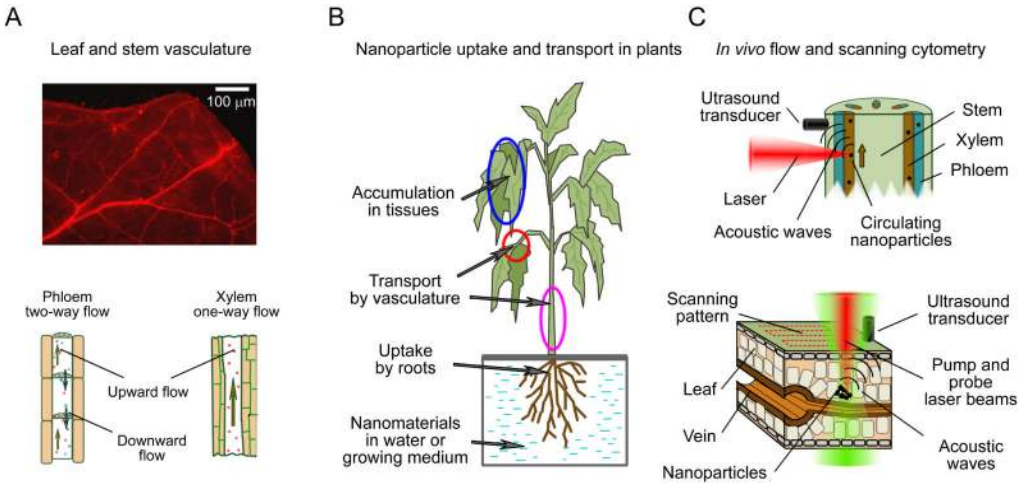

Figure 1.

Principles of *in vivo* plant cytometry. (**A)** Vascular vessels in a tomato leaf (top, autofluorescence, excitation 450 ± 40 nm, emission 600 ±8 nm) and schematics of flow in main plant vascular tissues (bottom). (**B)** Scheme of uptake, transport, and accumulation of nanomaterials from water or growing medium. (**C)** Principles of *in vivo* PA plant flow cytometry in a stem (top) and of *in vivo* PT/PA scanning plant cytometry in a leaf (bottom).

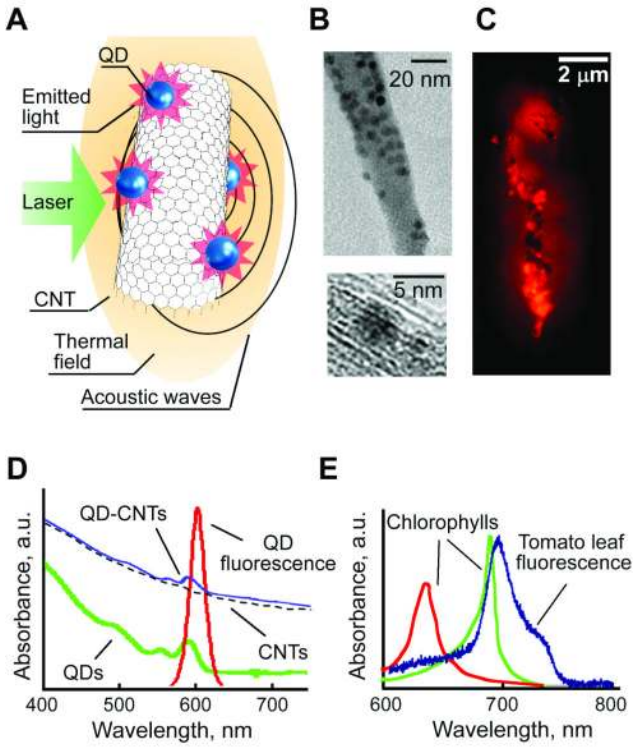

Figure 2.

QD-CNTs as multimodal PT, PA, and fluorescence contrast agents. **(A)** Schematic of laser-induced phenomena in QD-CNTs. (**B**) TEM image of multiple QDs on a CNT surface. (**C**) Fluorescent image of a QD-CNT cluster (excitation 450 ± 40 nm, emission 600 ±8 nm). (**D**) Absorption spectra of QDs, CNTs, QD-CNTs, and QD emission spectrum. (**E**) Auto-fluorescent spectra of a tomato leaf compared to typical absorption spectra of chlorophylls.

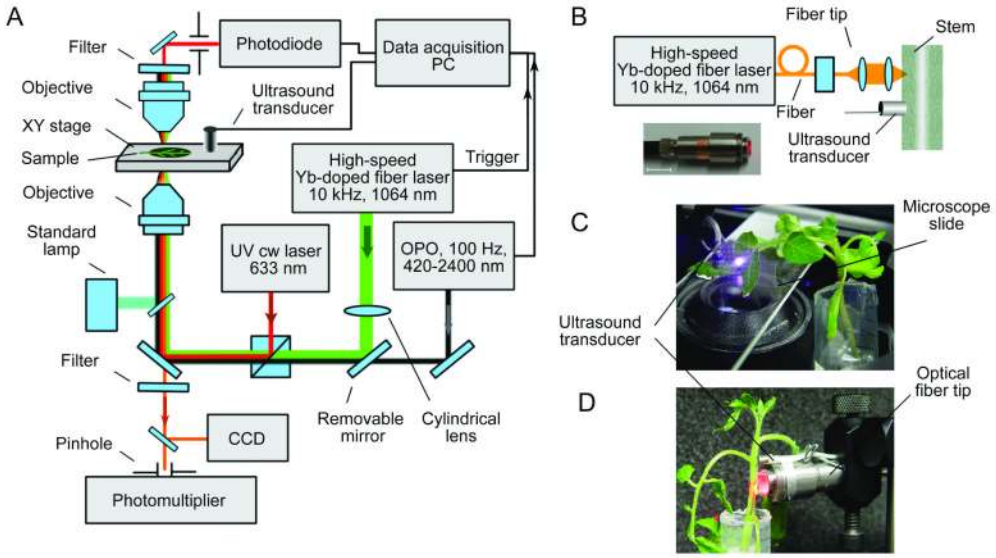

Figure 3.

In vivo integrated flow and scanning cytometry with PT, PA, and fluorescent detection schematics. (**A)** Schematic of the integrated setup. **(B)** Customized optical fiber tip for laser radiation delivery to plants. **(C)** Scanning cytometry in a leaf with the microscope schematic. (**D)** Optical fiber-based flow cytometry.

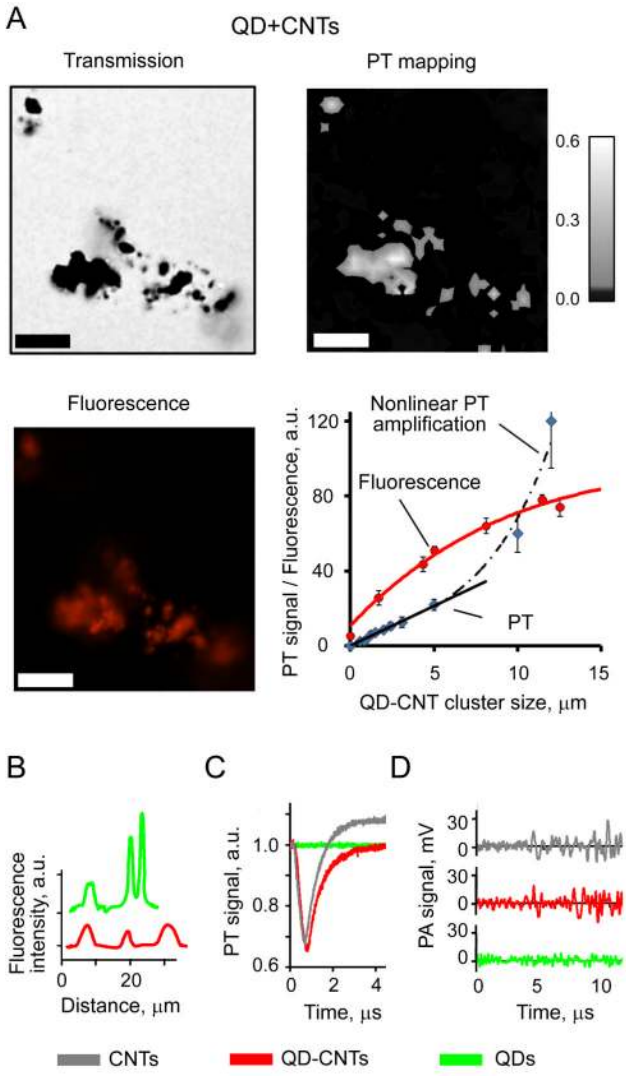

Figure 4.

In vitro detection and imaging of individual QDs, CNTs, and QD-CNTs. (**A**) Transmission (enhanced contrast), PT, and fluorescent imaging of QD-CNTs. Laser parameters: energy fluence of 0.05 J/cm^2, wavelength 903 nm, scan step 1 μm. Scale bar – 5 μm. Exposure of fluorescence imaging 200 ms. (**B**) Line profile for fluorescent intensity of 5 μm QD and QD-CNT clusters. (**C**) PT and (**D**) PA signals from ~1 μm QD, CNTs, and QD-CNT clusters: 903 nm, 0.05 J/cm^2.

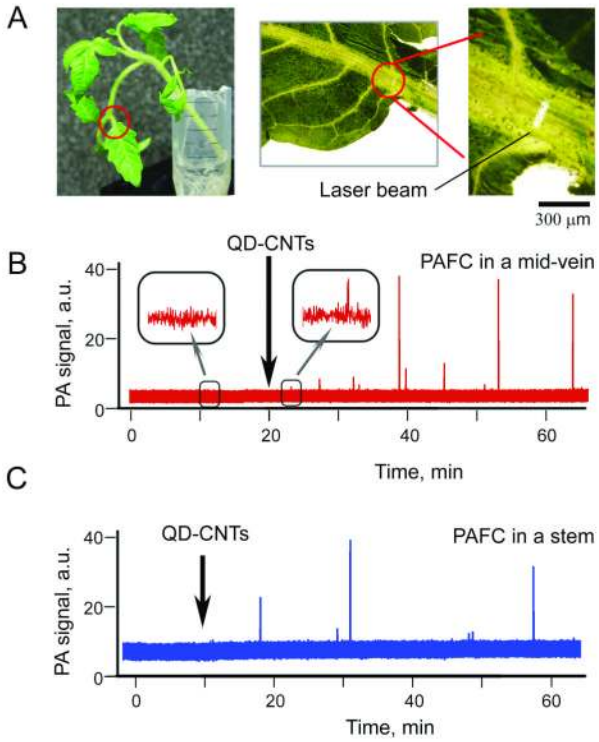

Figure 5.

In vivo PA plant flow cytometry of QD-CNTs in tomato vasculature. (**A)** Linear laser spot in a leaf mid-vein close to petiole. Red lines denote the part of the plant used for monitoring. **(B)** The trace of PA signals recorded in mid-vein after QD-CNTs were introduced into the water tank. Insets demonstrate enlarged parts of the control trace and the trace with small signal from QD-CNTs. (**C)** The trace of PA signals from QD-CNTs recorded in the stem (Fig. 3D). Black arrows indicate moment QD-CNTs were introduced into the water tank; the PA traces before introduction of QD-CNTs represent control data. Laser parameters: wavelength, 1064 nm; pulse width, 10 ns; pulse repetition rate, 10 kHz; laser pulse energy, 20 μJ; laser spot size in sample: 50×150 μm (**B**) and 100×400 μm (**C**).

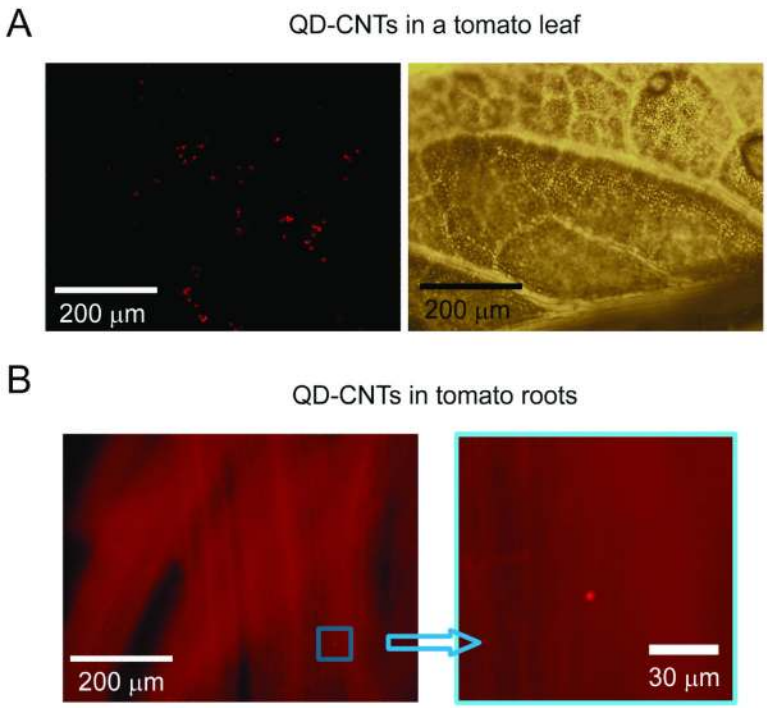

Figure 6.
Imaging of QD-CNTs in tomato tissues. (**A**) Fluorescent (left, exposure 100 ms, enhanced contrast) and transmission (right) images of a tomato leaf with accumulated QD-CNTs. (**B**) Fluorescent imaging of tomato roots: image at right magnifies part of the left image (exposure 5 s, no contrast enhancing).

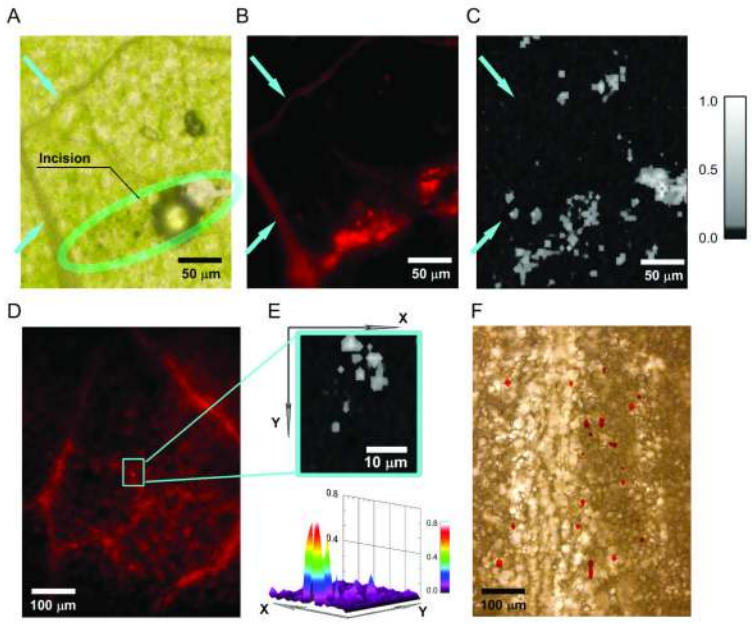

Figure 7.

Integrated scanning cytometry of QD-CNTs in tomato leaf using PT, PA, and fluorescent detection methods. (**A,B,C)** Transmission, fluorescence (enhanced contrast), and PT images (903 nm, 1.0 J/cm^2) of tomato leaf with the artificially introduced QD-CNTs. Blue arrows indicate leaf vascular tissues; green arrows mark position of the air bubble artifact. Fluorescent imaging exposure 200 ms. (**D, E)** Fluorescent and PT images of a leaf from 10-day-old tomato plant grown on a QD-CNT containing medium; exposure 200ms, enhanced contrast. (**F**) Transmission image of a sample having no distinctive fluorescence features overlaid with PT image (red) indicating locations of QD-CNTs.

Table 1

Potential applications for PT/PA scanning and flow cytometry in plants. Comparison with existing methods.

Application	Method	In vivo analysis	Simplicity of sample preparation	Mapping / localization	High sensitivity	Limitations	Refs.
Detection of nanomaterials accumulated in plants	Volume analysis after acid digestion	–	–	–	+	Sample destruction	(8,9,13)
	Optical transmission microscopy	–	+	+	±	Low depth	(9,16)
	Electron microscopy	–	–	+	+	Complex sample preparation	(9,14-16)
	MRI	+	+	+	–	Only magnetic materials.	(15)
	Raman and FTIR spectroscopy	+	+	–	–	Low sensitivity, large sample volumes	(9)
	PA/PT scanning microscopy	+	+	+	+	Absorbance background and light scattering in thick tissues	
Monitoring of nanomaterials uptake	Sampling different plants at selected time intervals, ex vivo analysis (see methods above)	–	–	+	±	Multiple biological replicates. Low time resolution. Invasive sampling.	(9)
	PA flow cytometry	+	+	+	+	Absorbance background and light scattering in thick tissues	
Viruses and pathogens, theranostics in xylem/phloem flow	Immunofluorescence microscopy	+	+	+	+	Autofluorescent artifacts.	(58)
	ELISA of xylem sap, ex vivo	–	–	–	+	Invasive sap extraction.	(59)
	PT detection and eradication with molecular labeling	+	+	+	+	Requires labeling of viruses and pathogens	(21,23)
Xylem/phloem transport studies	MRI	+	+	+	+	Low spatial resolution.	(17)
	Pressure probes	+	–	–	+	Invasive procedure.	(60)
	Radioisotope labeling	+	+	–	–	Radioactive probes.	(61)
	PA flow cytometry of contrast agents	+	+	+	+		